 doi:10.20944/preprints202203.0340.v1

Article

Monte Carlo simulations of the metal-directed self-assembly of Y-shaped positional isomers

Karolina Nieckarz [1] and Damian Nieckarz [2,*]

[1] Faculty of Chemistry, Maria Curie-Skłodowska University in Lublin, Maria Curie-Skłodowska Square 3, 20-031 Lublin, Poland; e-mail: kg.nieckarz@gmail.com

[2] Department of Theoretical Chemistry, Institute of Chemical Sciences, Faculty of Chemistry, Maria Curie-Skłodowska University in Lublin, Maria Curie-Skłodowska Square 3, 20-031 Lublin, Poland; e-mail: damian.nieckarz@poczta.umcs.lublin.pl

* Correspondence: e-mail: damian.nieckarz@poczta.umcs.lublin.pl; Tel.: +48 081 537 56 92

Abstract: The rational fabrication of low-dimensional materials with a well-defined topology and functions is an incredibly important aspect of nanotechnology. In particular, the on-surface synthesis (OSS) methods based on the bottom-up approach enable facile construction of sophisticated molecular architectures unattainable by traditional methods of wet chemistry. Among such supramolecular constructs especially interesting are surface-supported metal-organic networks (SMONs), composed of low-coordinated metal atoms and π-aromatic bridging linkers differing in size, shape and functionalization scheme. In this work, the lattice Monte Carlo (MC) simulation technique was used to extract the chemical information encoded in a family of Y-shaped positional isomers coadsorbed with trivalent metal atoms on a flat metallic surface with (111) geometry. For this purpose the investigated tritopic molecules/metal atoms were carefully mapped on a triangular lattice as interconnected/isolated segments with appropriatelly embedded anisotropic interactions. Depending on the intramolecular distribution of active centers (functional groups) within the simulated molecular bricks, we observed the metal-directed self-assembly of two-dimensional (2D) openwork patterns, aperiodic mosaics and metal-organic ladders. The obtained theoretical findings could be especially relevant for the scanning tunneling microscopy (STM) experimentalists interested in a surface-assisted construction of complex nanomaterials stabilized by directional coordination bonds.

Keywords: Monte Carlo simulations; self-assembled overlayers; openwork structures; surface nanopatterns; positional isomers

1. Introduction

In arts and crafts, the openwork ornamentation is particularly popular, which consists in cutting holes with well-defined geometrical shapes in a preselected material (fabric, clay, wood, etc.). Thanks to the holes, a beam of light is introduced into the artistic composition, which shapes the object with a play of chiaroscuro and subtly emphasizes its fragile internal structure [1]. Interestingly, many one-atom-thick molecular assemblies like surface-supported metal-organic networks (SMONs) exhibit a non-trivial, openwork structure [2-7]. This is due to the presence of empty cavities (nanopores) within their structure that could differ in shape, spatial distribution, and chirality [8-10]. Moreover, the openwork supramolecular architectures stabilized by directional ligand→metal coordination bonds are not only aesthetically pleasing but could also find practical appli-

 doi:10.20944/preprints202203.0340.v1

cations in nanotechnology (as selective molecular sieves, atomically defined adsorbents, surface protective coatings, etc.), nanotribology, and heterogeneous catalysis [11-14].

To date, numerous molecular precursors with a different symmetry, predefined shape, size and intramolecular distribution of functional groups have been synthesized and successfully applied as building blocks of plethora SMONs with tailorable morphology, porosity and functions [2, 4, 5, 9, 11, 15-19]. Among them, especially prominent is a family of small star-shaped molecules with C_3-symmetrical backbone, comprising interconnected phenyl moieties. In the last decades, such carbon-based molecular bricks made possible the on-surface synthesis (OSS) of diverse metal-organic networks [4, 13, 16, 18, 19-22], sophisticated planar tessellations [23], ladders [24], nanoribbons and small isolated aggregates [25, 26]. However, much less attention was paid to the analogous carbon-based molecules with a reduced symmetry so far [27-29]. For these molecular building blocks, the outcome of metal-directed self-assembly is usually hard to predict. It is especially true in the case of conformationally flexible molecules with a high structural heterogeneity, whose terminal phenyl moieties are differently functionalized [30].

In our previous work, we have demonstrated that the tripodal ligands with properly assigned interaction centers could be valuable building blocks of the novel metal-organic architectures [31]. However, the performed computer simulations were limited only to the molecular bricks with C_3-symmetrical backbone. Therefore, in this contribution, we extend our theoretical investigations on a family of Y-shaped positional isomers whose arms differ in length and are equipped with active centers (functional groups) embedded in *para* and/or *meta* positions. To that end, we have applied a classical lattice Monte Carlo (MC) method, which allows for a comprehensible investigation of complex molecular assemblies [32-34]. Moreover, the lattice MC simulations based on discrete intermolecular potentials enable avoiding tedious, time-consuming force calculations [35, 36]. The main objective of our work is to extract the chemical information encoded in the studied molecules and exploit the gained hints to steer the morphology of surface-confined patterns, comprising Y-shaped bridging linkers and trivalent metal atoms. The obtained results could be especially useful in the context of surface-assisted fabricated of novel openwork nanomaterials, metal-organic ladders, and aperiodic mosaics with untrivial topologies.

2. Materials and Methods

To explore the surface-supported self-assembly of positional isomers **A**-**J** (see Figure 1) the coarse-grained Monte Carlo (MC) simulations were performed in the NLT ensemble, where $N = l + m$ means the total number of adsorbed entities (where $l = 600$ is the number of Y-shaped ligands and $m = l$ metal atoms), L stands for the linear size of the simulated system ($L = 130$), and T is temperature. The MC computer calculations were performed on a rhombic fragment of flat triangular lattice comprising $L \times L$ energetically equivalent adsorption sites (vertices of a triangular lattice) at low surface coverage, defined as $\theta = (5l + m)L^{-2}$ (if not stated otherwise). In the adopted model the two-dimensional (2D) triangular lattice represents atomically smooth crystalline M(111) surface with no defects and corrugations, where M = Cu, Ag or Au. The distance between two neighboring adsorption sites on a triangular lattice was arbitrary set to 1, and expressed in dimensionless units, for the sake of simplicity. To minimize the influence of negative edge-effects on the morphology of resulting molecular patterns, the periodic boundary conditions in all planar directions of 2D lattice were imposed. Additionally, to avoid formation of unwanted point structural defects (missing ligands/metal atoms, self-interstitial defect, etc.), the annealing procedure was applied. Namely, the simulated overlayer was linearly cooled down form the initial temperature $T = 1.001$, to the target temperature $T = 0.001$ in 10^3 equal intervals $dT = 0.001$, comprising $6N \cdot 10^3$ MC

Preprints (www.preprints.org) | NOT PEER-REVIEWED | Posted: 25 March 2022 doi:10.20944/preprints202203.0340.v1

steps, each (one MC step is a single displacement/in-plane rotation trial of randomly selected entity adsorbed on a triangular lattice).

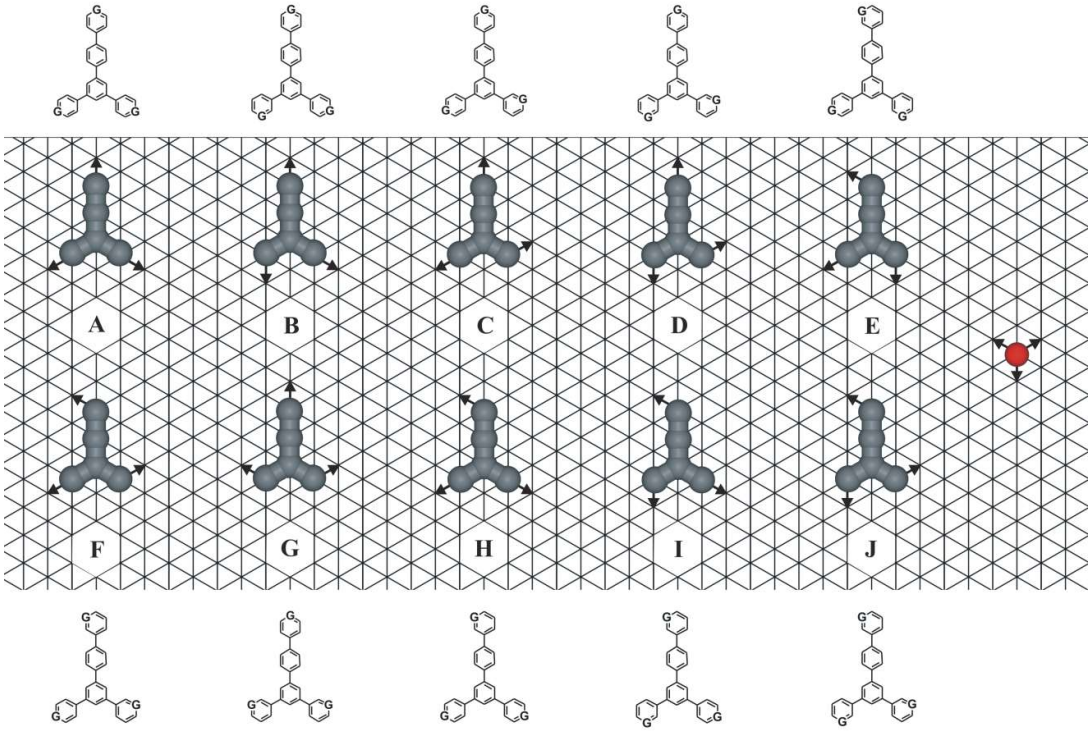

Figure 1. A survey of Y-shaped positional isomers **A**-**J** and their modeled counterparts adsorbed on a triangular lattice. The black arrows attached to the terminal segments of the simulated molecules denote positions of active centers (functional groups of real organic molecules: G = nitrile/propiolonitrile moiety, ring-nitrogen atom), able to interact reversibly with coadsorbed trivalent metal atom (red, isolated segment). For clarity, in the case of prochiral units (**B**-**F** and **H**-**J**) only one surface isomer, denoted arbitrary as (*S*) is shown. The vertices of a triangular lattice represent isolated adsorption sites present in an energetically homogenous metallic surface with (111) geometry.

The MC simulations started with a random distribution of l tripodal ligands (linkers) and m trivalent metal atoms on a triangular lattice in an optimal $l/m = 1{:}1$ stoichiometric ratio. Then, in the next step the investigated metal-organic overlayer was energetically equilibrated in a series of $6N \cdot 10^6$ MC steps. For this purpose, one component of the adsorbed overlayer was selected at random, and its total potential energy E_1 was determined. Then, the chosen ligand/metal atom was displaced within the 2D lattice or rotated in place (only if the Y-shaped molecule was selected) by a magnitude of acute angle ± 60. If this operation was successful, its total potential energy E_2 in a new position Ω was calculated. Otherwise, the tested entity was left in the original configuration on a lattice, and the above outlined procedure was successively iterated. The ligand/metal atom displacement attempt was accepted/rejected based on the Metropolis MC criterion [37, 38], involving calculation of transition probability $p = min\{1, exp(-\Delta E/k_B T)\}$, where $\Delta E = E_2 - E_1$ is the potential energy difference between the new and the old position of the probed entity, k_B denotes reduced Boltzmann constant ($k_B = 1$ in our model) and T is a system temperature. In the case $E_2 \leq E_1$ the new position Ω was accepted unconditionally. Otherwise, the random number $r \in (0,1)$ was generated and compared with a transition probability p. If a random number r satisfied

 doi:10.20944/preprints202203.0340.v1

inequality $r \leq p$, the new position Ω was accepted. In the latter case ($r > p$), the tested configuration was rejected, and ligand/metal atom was moved back to the original position on a triangular lattice.

In the adopted theoretical model each of the π-aromatic positional isomers **A**-**J** is represented by a group of in-plane interconnected hard spheres (segments) with properly assigned active centers (black arrows in Figure 1), while metal atoms are modeled as single flat segments. In our coarse-grained approach, a single gray segment corresponds to one phenyl ring of real surface isomer **A**-**J**, while segment-segment connections represent C-C sigma bonds linking aromatic moieties of the studied molecules. Additionally, each gray segment present within the simulated linker **A**-**J** covers only one adsorption site on a triangular lattice (localized, monolayer adsorption). The same is true in the case of a single metal atom. Contrary to the classical Langmuir adsorption model, desorption of components of the investigated metal-organic overlayers is prohibited (NLT ensemble). Moreover, lateral interactions between physisorbed Y-shaped ligands and metal atoms on the adjacent adsorption sites of a triangular lattice are possible: the in-plane ligand→metal interactions were assumed to be short-ranged (limited to the neighboring adsorption sites on a lattice), anisotropic, equal in strength ($\omega = -1.0$, negative value means attraction), and reversible. We assumed that a single coordination bond could be formed only if the metal atom m and linker l met on a triangular lattice in a proper spatial configuration: one of the outer segments of Y-shaped linker and metal atom cover two adjacent adsorption sites (vertices of a triangular lattice), and assigned to them interaction directions (black arrows) are oppositely directed (→←), and collinear. To solely extract the chemical information encoded in the geometric shape and intramolecular distribution of active centers of the positional isomers **A**-**J**, we assumed that the potential energy of anisotropic coordination bond prevail over other interactions possible in the studied metal-organic overlayers. For this purpose, all potential energies associated with the ligand↔surface, metal↔surface, metal↔metal, and ligand↔ligand side-to-side interactions were set to zero. Additionally, to compare the structural properties of the ordered 2D metal-organic patterns, we introduced the structural parameter called density ρ. This dimensionless parameter was defined as the ratio of occupied adsorptions sites inside a unit cell of arbitrary selected phase and the total area A of this unit cell, that is $\rho = (5xl + ym)A^{-1}$, where x and y denote the number of linkers l, and metal atoms m within unit cell, respectively.

3. Results and discussion

Initial MC simulations were conducted for the C_1-symmetric positional isomer **A**, which arms are functionalized exclusively in para positions. Such intramolecular distribution of identical active centers makes linker **A** achiral, which manifests in a relatively simple morphology of the emerging supramolecular patterns. However, even such trivial functionalization scheme combined with a reduced symmetry of molecule **A** directed the surface-confined self-assembly into two polymorphic superstructures with distinct morphological properties like density ρ, pore size/shape, and their spatial distribution (see Figures 2a-b).

Preprints (www.preprints.org) | NOT PEER-REVIEWED | Posted: 25 March 2022 doi:10.20944/preprints202203.0340.v1

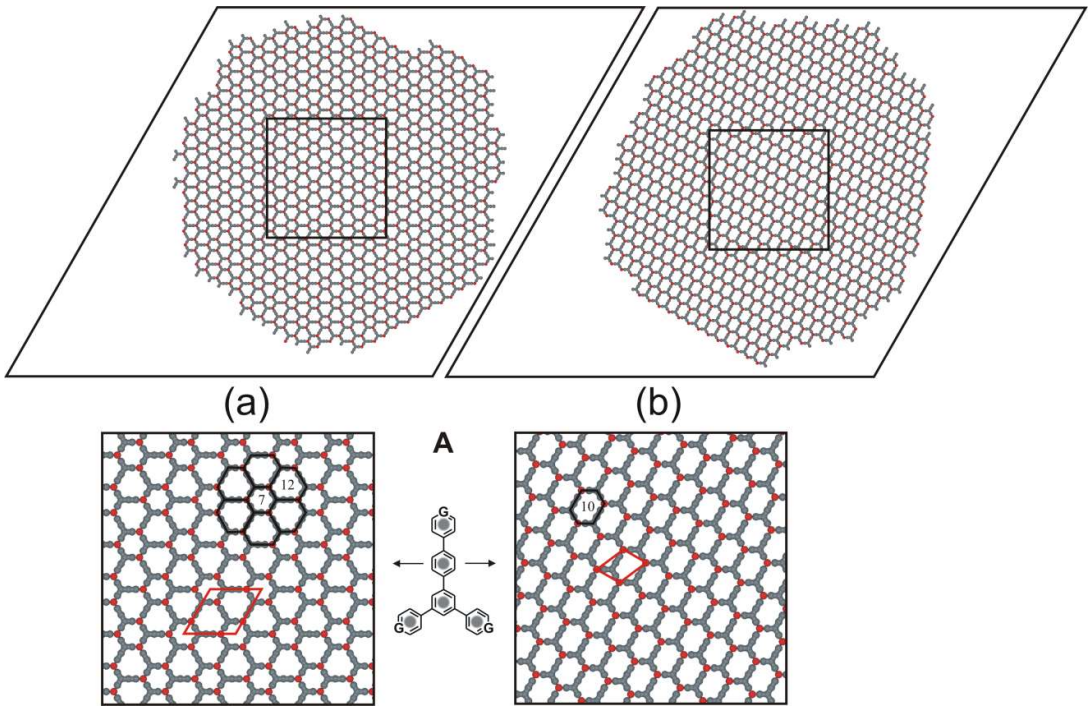

Figure 2. (**a**) The open porous metal-organic network composed of 600 metal atoms (red isolated segments) and 600 achiral ligands **A** in optimal 1:1 stoichiometric ratio at surface coverage $\theta \sim 0.21$, $T = 0.001$; (**b**) Homogenous brick wall-like overlayer comprising 600 metal atoms and 600 molecules **A** at surface coverage $\theta \sim 0.21$, $T = 0.001$. In the magnified fragments of the corresponding phases the rhombic unit cells are marked (solid red lines). The solid black lines mark the edges of empty pores differing in size and shape. Inside the highlighted nanopores the numbers of empty adsorption sites are given. The vertices of a triangular lattice (adsorption sites) are not shown for the sake of clarity.

As it is seen in Figure 2a, the first polymorph ($\rho = 0.371$) is characterized by a rhombic unit cell (7×7, $\angle 60/120^o$) comprising 3 linkers **A** and 3 metal atoms in 1:1 stoichiometric ratio. The cavities present within the corresponding network are periodically distributed and arranged into a flower-like pattern with central hexagonal void (7 adsorption sites), and six petals (12 adsorption sites, each) with the shape of a truncated equilateral triangle. In comparision to the discussed phase, the brick wall-shaped polymorphic network shown in Figure 2b has a ~15% higher density ($\rho = 0.433$). Its parallelogram unit cell ($2\sqrt{3} \times \sqrt{19}$, $\angle 67/113^o$), contains only one linker **A** and one metal atom. Moreover, all Y-shaped ligands **A** present within this homogenous superstructure are oriented unidirectionally. The adjacent pores are also oriented along the same direction of a triangular lattice and comprise 10 adsorption sites, each. Although the discussed 2D polymorphs are almost energetically equivalent, the surface-confined self-assembly of a heteroporous network illustrated in Figure 2a is privileged due to entropic reasons. Namely, after visual inspection of 50 independent system replicas, it revealed that the two-porous phase was formed selectively in ~66% of them. This result could be reasonably explained comparing the number of spatial orientations of linkers **A** within the polymorphic phases - in the superstructure shown in Figure 2a each bridging linker **A** could be incorporated into the growing metal-organic network in three different ways, whereas in the case of uniporous network (Figure 2b) only unidirectional arrangement of ligands **A** could result in not disturbed formation of a defect-free overlayer. Interestingly, similar crystalline polymorphs were observed experimentally in the case of 3,3′,5,5′-tetrabromo-2,2′,4,4′,6,6′-hexafluorobiphenyl (Br_4F_6BP) molecules [39], brominated tetrathienoanthracene [40], as well as modeled theoretically [41]. In the light of the

Preprints (www.preprints.org) | NOT PEER-REVIEWED | Posted: 25 March 2022 doi:10.20944/preprints202203.0340.v1

above-listed scientific reports, the discussed two-directional self-assembly is no exception but rather the next example of dichotomous formation of complex metal-organic patterns.

Contrary to the achiral molecule **A**, the next studied positional isomer **B** is functionalized at one (*S*)-*meta* and two *para* positions. As shown in Figure 3a, this intramolecular distribution of active centers (functional groups G) allows for a highly selective formation of the openwork metal-organic network with huge cavities (55 adsorption sites) surrounded concentrically by smaller pores comprising 12 and 2 adsorption sites, each. The gear-like shaped voids have diameter $d = 8$ (corner-to-corner) and unique set of teeth differing in length, that is $(1.1.3)^6$. In the adopted notation individual number denotes the length of a single tooth, while the number sequence corresponds to their order of occurrence at the edges of the largest pore. The characteristic feature of the heteroporous phase is a relatively low density $\rho = 0.344$ and exceptionally large rhombic unit cell $(11 \times 11, \angle 60/120^{o})$, comprising 6 molecules **B** and 6 metal atoms in 1:1 stoichiometric ratio.

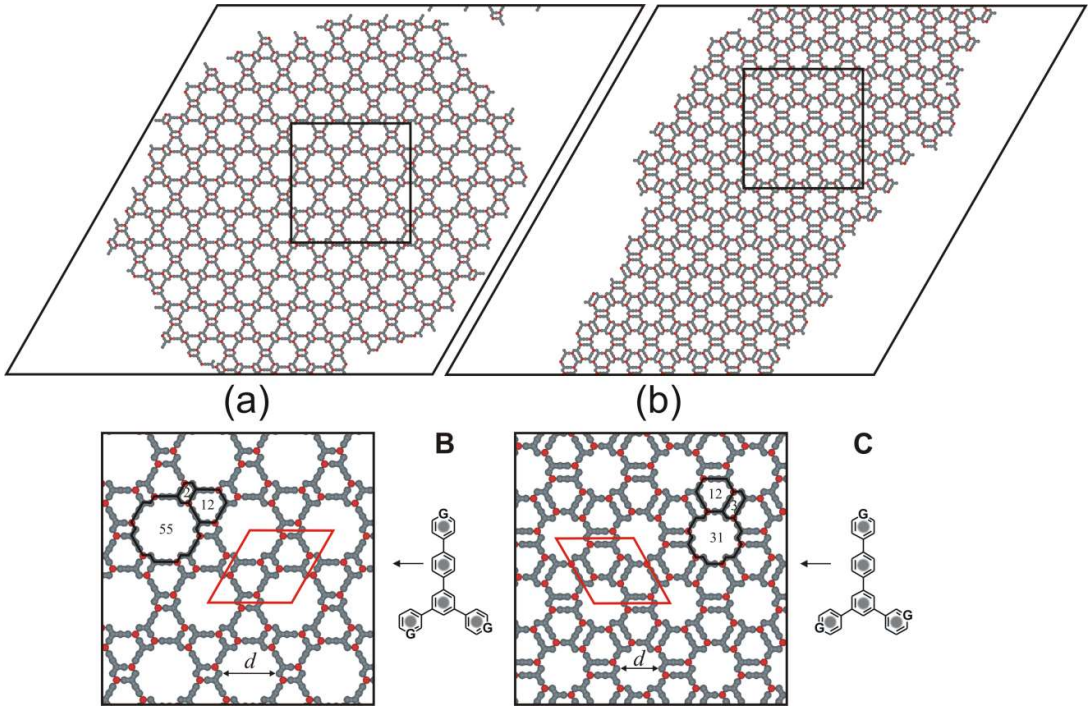

Figure 3. (**a**) Multiporous metal-organic network composed of 600 metal atoms and 600 ligands **B** in 1:1 stoichiometric ratio; (**b**) Openwork phase comprising 600 metal atoms and 600 ligands **C**. In the magnified fragments of the metal-organic patterns rhombic unit cells are marked (solid red lines). The solid black lines mark the edges of nanopores differing in size and shape. Inside the highlighted nanopores the numbers of empty adsorption sites are given. For the largest gear-like shaped nanopores their diameters d (corner-to-corner) are marked.

Embedding an active center on the second short arm of tritopic molecule **B** in (*S*)-*meta* position gives a subsequent positional isomer, denoted by the letter **C**. In this molecule the (*S*)-*meta* active center is pointed towards its long arm monofunctionalized in *para* position. Interestingly, even such tiny structural modification strongly affects the topology of the resulting supramolecular network. As illustrated in Figure 3b, the infinite metal-organic phase exhibits basic structural features of the adsorbed overlayer from Figure 3a. The gear-like shaped voids $(1.1.2)^6$ of the considered superstructure encompass 31 adsorption sites and are separated by adjacent small pores comprising 12 and 3 free adsorption sites. Additionally, with a relatively small diameter of the largest pores

Preprints (www.preprints.org) | NOT PEER-REVIEWED | Posted: 25 March 2022 doi:10.20944/preprints202203.0340.v1

($d = 6$) follows substantial density increasing of the crystalline structure ($\rho = 0.416$), as well as side length reduction of its unit cell (10×10, $\angle 60/120^{o}$). Surprisingly, displacement of the *para* active center attached to the short arm of linker **C** to the (*S*)-*meta* position (within the same outer segment), had directed the metal-assisted self-assembly into subsequent open porous network (see Figure 4a) with vast cavities, characteristic for the overlayer illustrated in Figure 3a. However, within the discussed adlayer the gear-like shaped voids $(1.1.2)^{6}$ are separated by alternatively arranged small pores with a star-shaped (4 adsorption sites) and needle-like geometry (3 adsorption sites). The rhombic unit cell of the corresponding supramolecular structure contains 6 surface isomers **D** and 6 metal atoms in 1:1 stoichiometric ratio.

In contrast to the above-discussed molecular assemblies, in the case of isomer **E**, which arms are functionalized in different positions: in *para*/(*R*)-*meta*/(*S*)-*meta* mode counting anticlockwise; we have not observed emerging an open porous phase with translational symmetry. Instead, the isolated metal-organic ladders were obtained. In the exemplary snapshot shown in Figure 4b, each ladder comprises alternately arranged small pores comprising 4 and 2 adsorption sites, while the metal atoms incorporated into its structure are arranged in a zig-zag fashion (blue line in a magnified fragment of Figure 4b). Although the metal-organic ladders are randomly distributed on a triangular lattice, all of them are pointed unidirectionally. Such preferred spatial configuration is not surprising, as provides unperturbed elongation (metal-directed growth) of individual ladders.

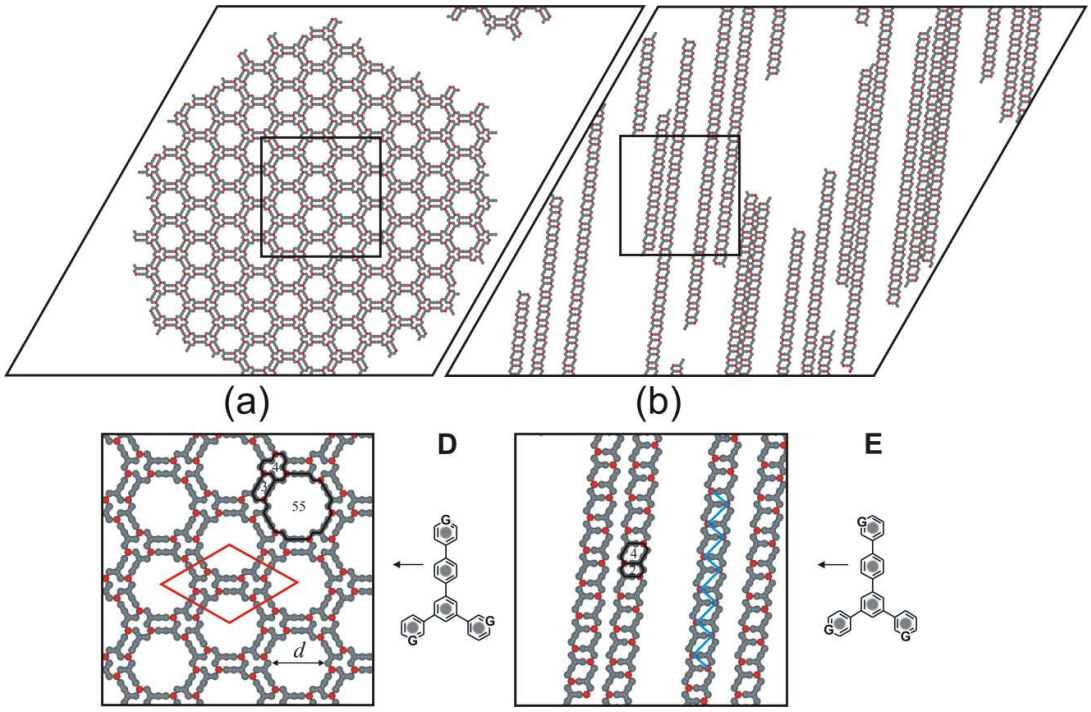

Figure 4. (**a**) Highly crystalline metal-organic phase composed of 600 metal atoms and 600 ligands **D** in 1:1 stoichiometric ratio; (**b**) adsorbed overlayer comprising 600 metal atoms and 600 ligands **E** in 1:1 stoichiometric ratio. In a magnified fragment of the open porous network a rhombic unit cell is marked (solid red line). The solid black lines mark the edges of empty nanopores differing in size and shape. Inside the highlighted nanopores the numbers of empty adsorption sites are given. The solid blue line denotes the zig-zag pattern created by metal atoms cementing metal-organic ladder.

As shown in Figure 5a also in the case of positional isomer **F**, the obtained metal-organic phase differ largely in morphology from the supramolecular architectures depicted in Figures 2-4a. Namely, its main feature is a lack of translational order. As shown

Preprints (www.preprints.org) | NOT PEER-REVIEWED | Posted: 25 March 2022 doi:10.20944/preprints202203.0340.v1

in the magnified fragment of Figure 4a the multiporous phase is built of three types of empty cavities marked in different colors: pink (10 adsorption sites), chalk (7 adsorption sites), and light-green (4 adsorption sites). Interestingly, the basic morphological properties of the considered overlayer are also conserved at two times higher surface coverage (see Figure 5b).

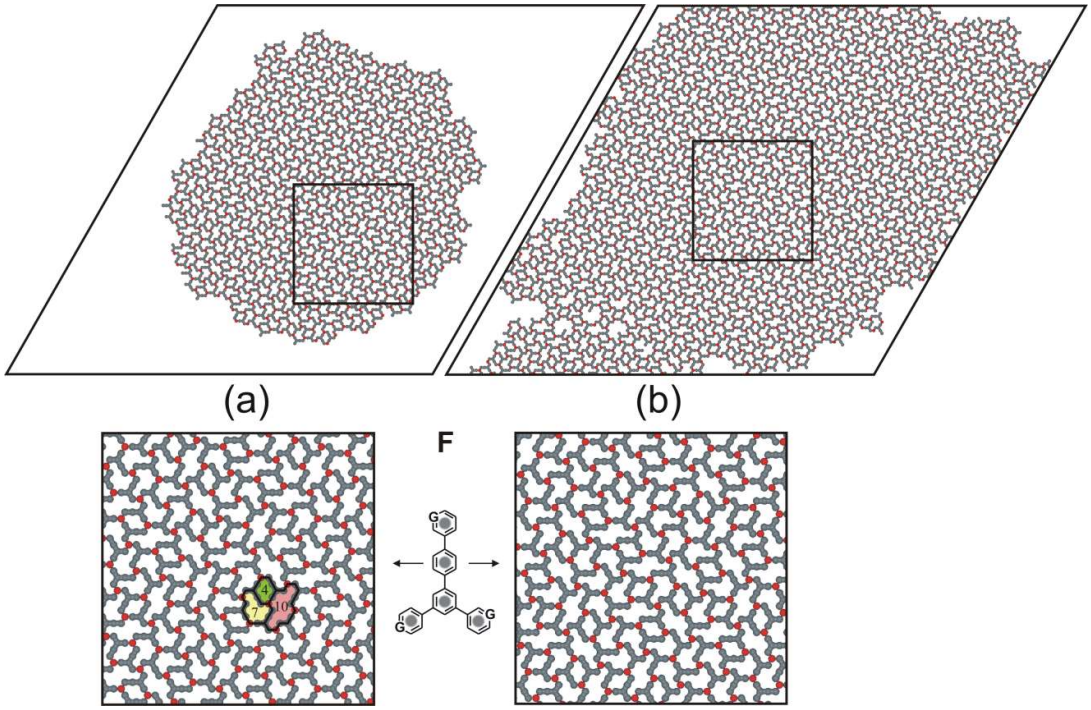

Figure 5. (**a**) Exemplary aperiodic metal-organic network composed of 600 metal atoms and 600 ligands **F** in 1:1 stoichiometric ratio at surface coverage $\theta \sim 0.21$, $T = 0.001$; (**b**) Adsorbed overlayer comprising 1200 metal atoms and 1200 ligands **F** in 1:1 stoichiometric ratio at surface coverage $\theta \sim 0.42$, $T = 0.001$. The solid black lines in the bottom-left inset mark the edges of empty nanopores differing in size and shape. Inside the highlighted nanopores the numbers of empty adsorption sites are given.

The aperiodicity of the overlayers shown in Figures 5a-b originates exclusively from not regular distribution of bridging linkers **F**, whereas trivalent metal atoms occupy vertices of a well-defined triangular lattice with a primitive unit cell (see Figure 6b). Other unique feature of the aperiodic mosaics from Figures 5a-b are randomly distributed flower-like rosettes with closed and open walls. As shown in the magnified fragment of Figure 6a, the central point of a closed hexagonal rosette is a windmill-like three-fold coordination node surrounded by two coordination shells comprising a periodical array of metal atoms and molecules **F**. However, this perfect spatial arrangement of bridging linkers/metal atoms could be easily perturbed without generation any point structural defects. Therefore, in the mosaic superstructure many open-walled rosettes could be easily identified. Within the aperiodic metal-organic network from Figure 5a, the most abundant are irregular pores marked in chalk color (~ 50%), while the light-green and pink elongated cavities are almost equally populated, and constitute ~ 27% and ~ 23% of all empty pores present in the considered overlayer (averages from 5 independent system replicas).

Preprints (www.preprints.org) | NOT PEER-REVIEWED | Posted: 25 March 2022 doi:10.20944/preprints202203.0340.v1

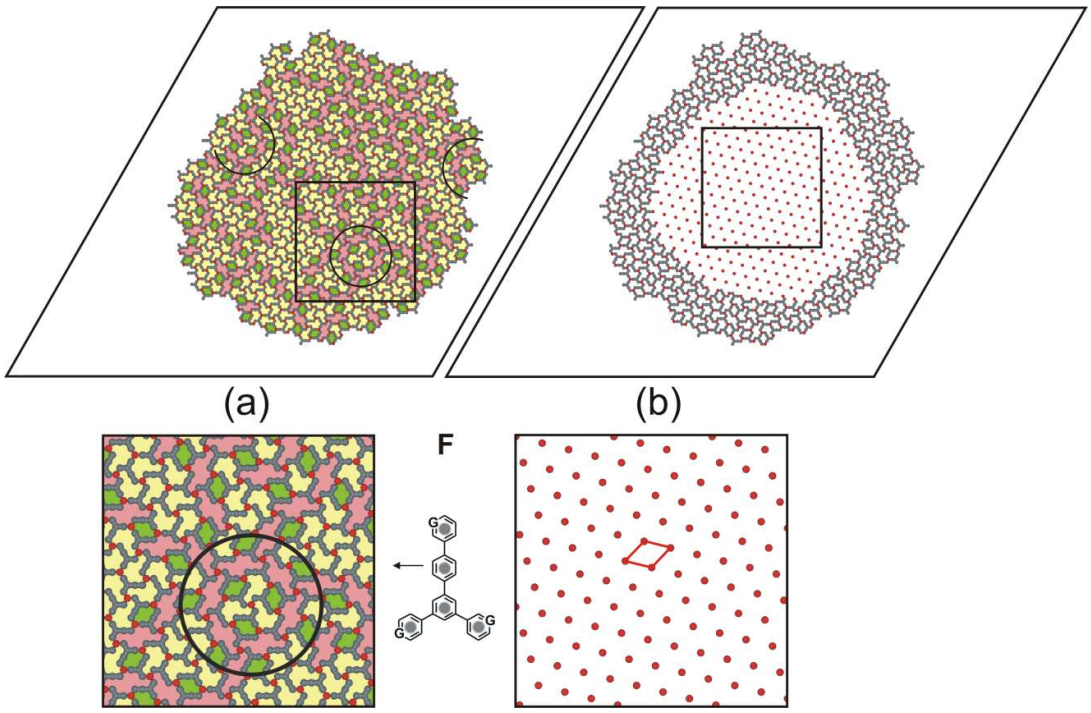

Figure 6. (**a**) The random distribution of nanopores within metal-organic network built of 600 metal atoms and 600 ligands **F**. The solid black oval in the magnified fragment of mosaic superstructure encompasses hexagonal closed rosette with a periodic arrangement of metal atoms and linkers **F**. The incomplete solid black ovals denote positions of open-walled rosettes; (**b**) Supramolecular phase from Figure 5a, were some bridging ligands **F** were removed to better visualize a highly periodic distribution of metal atoms (red isolated segments). The solid red line indicates a primitive rhombic unit cell ($\sqrt{13} \times \sqrt{13} \angle 60/120^{o}$).

Even after the cursory visual inspection of the aperiodic mosaics illustrated in Figures 5a-b, it becomes clear that the metal-directed self-assembly of molecules **F** could produce also other metal-organic patterns with a highly periodic distribution of bridging linkers **F** and metal atoms. Small fragments of such artificially created connections are shown in Figure 7. Among them, especially interesting are overlayers composed of flower-like rosettes (Figures 7a-b). The first of them ($\rho = 0.533$) is built of adjacent hexagonal rosettes with central windmill-like coordination nodes oriented clockwise (see Figure 7a). The second polymorph with a huge rhombic unit cell ($\sqrt{234} \times \sqrt{234} \angle 60/120^{o}$) also comprises closed hexagonal rosettes but some of their central windmill-like nodes are oriented anticlockwise (Figure 7b). Moreover, one could imagine a morphologically similar phase (with equal density ρ), where the windmill-like coordination nodes are randomly oriented. The third artificial overlayer shown in Figure 7c, resembles an open porous network obtained for molecule **C** (see Figure 3b). However, within this phase the gear-like shaped cavities $(1.1.2)^6$ with a diameter $d = 6$ (corner-to-corner) are surrounded concentrically by smaller pores comprising 4 and 6 adsorption sites. The last crystalline pattern is homogenous in terms of porosity ($\rho = 0.533$), and comprises only irregular voids containing 8 adsorption sites, each (Figure 7d).

Preprints (www.preprints.org) | NOT PEER-REVIEWED | Posted: 25 March 2022 doi:10.20944/preprints202203.0340.v1

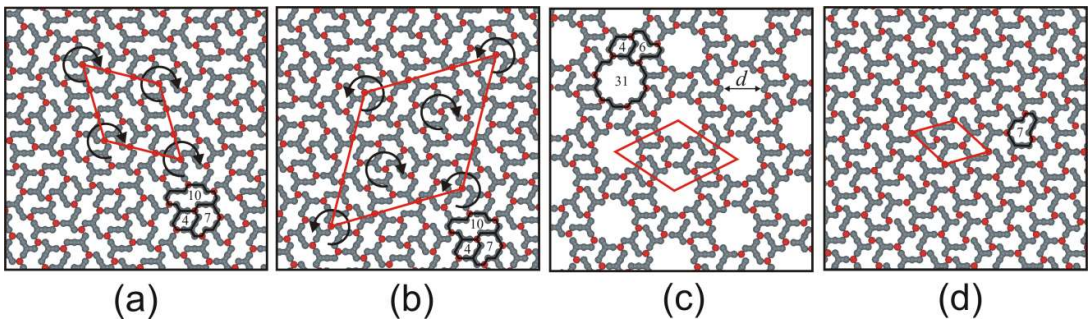

Figure 7. Small fragments of artificially created metal-organic overlayers composed of ligands **F** and trivalent metal atoms. The solid red lines delimit unit cells of the crystalline supramolecular patterns. The solid black lines mark the edges of empty nanopores differing in size and shape. Inside the highlighted nanopores the numbers of empty adsorption sites are given. (**a**-**b**) The flower-like networks with density $\rho = 0.533$ and rhombic unit cells differing in side lengths: $\left(\sqrt{117} \times \sqrt{117}\ \angle 60/120^{o}\right)$ and $\left(\sqrt{234} \times \sqrt{234} \angle 60/120^{o}\right)$. The black curved arrows denote a handedness of individual closed rosettes; (**c**) The multiporous phase with a rhombic unit cell $\left(\sqrt{91} \times \sqrt{91},\ \angle 60/120^{o}\right)$ and density $\rho = 0.457$; (**d**) The homoporous phase with a rhombic unit cell $\left(\sqrt{39} \times \sqrt{39},\ \angle 60/120^{o}\right)$ and density equal to $\rho = 0.533$.

The next studied molecule, denoted by a letter **G**, is characterized by a highly symmetrical distribution of active centers (see Figure 8). Namely, the long arm of anchor-like ligand **G** is equipped with an active center in the *para* position, whereas the remaining two shorter arms (equal in length) are functionalized in *meta* positions with an opposite in-plane orientations: (*R*) and (*S*). In consequence, both *meta* active centers are pointed to the *para* functionalized arm of C_1-symmetric molecule **G**. Such unique functionalization scheme allows this considered isomer self-assembly with trivalent metal atoms into a highly aperiodic superstructure with no structural defects (see Figure 8a). As shown in the magnified fragment of Figure 8a, the complex mosaic phase is composed of 6 different cavities. Among them are kite-like voids (○, ○-○, ○-○-○) encompassing 6, 12, and 18 free adsorption sites; elongated saw-like pores ● (9 adsorption sites), and ●-● (15 adsorption sites); and small needle-like voids •, comprising only 3 adsorption sites. Like in the case of mosaic overlayers depicted in Figures 5a-b, the aperiodicity of the considered metal-organic network originates only from not regular distribution of anchor-like linkers **G**, while the isolated metal atoms occupy vertices of a periodic triangular lattice with primitive unit cell $\left(2\sqrt{3} \times 2\sqrt{3},\ \angle 60/120^{o}\right)$. Surprisingly, at high surface coverage ($\theta \sim 0.53$), some fraction of molecules **G** is engaged in the formation of metal-organic ladders coexisting with an aperiodic phase (see Figure 8b). As shown in a magnified fragment of Figure 8b, the metal-organic ladders are close-packed and oriented along the same direction of a triangular lattice. However, the adjacent ladders comprising small needle-like voids • do not create a periodic crystalline phase, as some of them are translated in-plane with respect to the others. A closer visual inspection of an aperiodic superstructure shown in Figure 8a, reveals that similar ladder-like metal-organic connections are also present into its structure. However, the lengths of these ordered connections are relatively small - most of the metal-organic ladders incorporated into phase illustrated in Figure 8a comprise only from 2 to 5 parallel oriented linkers **G**.

Preprints (www.preprints.org) | NOT PEER-REVIEWED | Posted: 25 March 2022 doi:10.20944/preprints202203.0340.v1

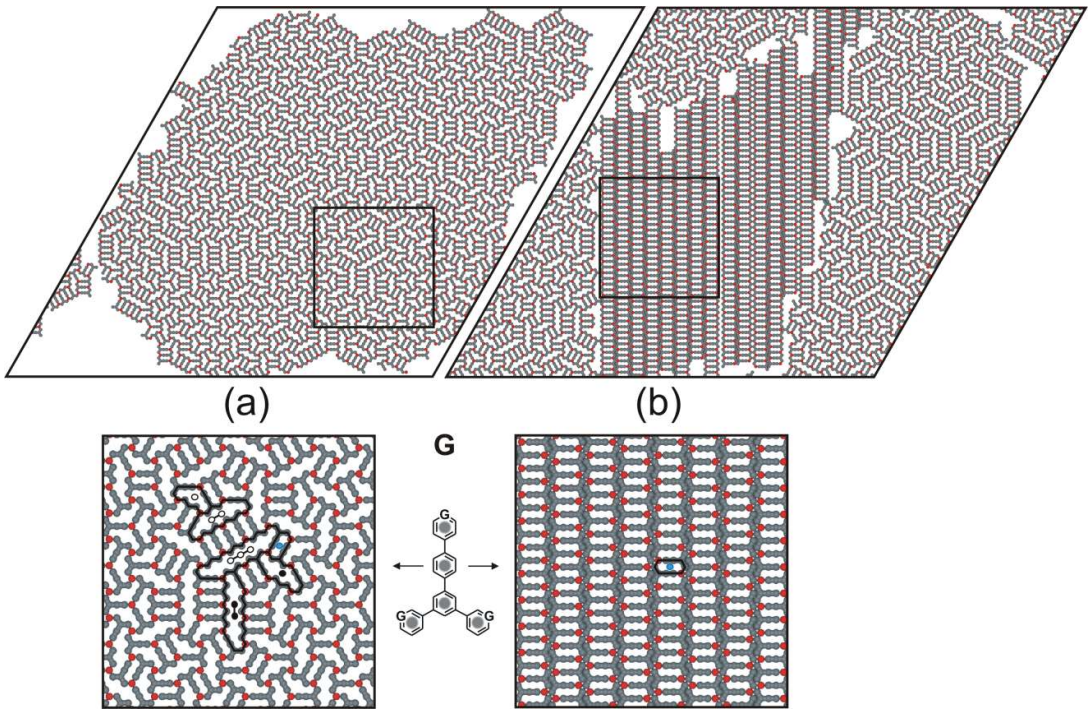

Figure 8. (**a**) The aperiodic metal-organic network comprising 1200 metal atoms and 1200 anchor-like ligands **G** in 1:1 stoichiometric ratio at surface coverage $\theta \sim 0.42$, $T = 0.001$; (**b**) Adsorbed overlayer composed of 1500 metal atoms and 1500 molecules ligands **G** in 1:1 stoichiometric ratio at surface coverage $\theta \sim 0.53$, $T = 0.001$. The solid black lines mark the edges of empty nanopores differing in size and shape.

Unlike aperiodic mosaics created by the positional isomers **F** and **G**, the supramolecular pattern obtained for molecule **H** is highly regular. As it is seen in Figure 9a the open porous network comprises three types of nanocavities. Among them are large gear-like shaped voids $(1.2.2)^6$ with a diameter $d = 2\sqrt{13}$ (corner-to-corner), hexagonal pores (7 adsorption sites), and truncated rhombus-like small voids (4 adsorption sites). Inside the rhombic unit cell $\left(\sqrt{111} \times \sqrt{111}, \angle 69/111^{o}\right)$ of the crystalline overlayer, there are 6 molecules **H** and 6 metal atoms. Moreover, the multiporous phase has low density $(\rho = 0.346)$, comparable with the metal-organic array composed of surface isomers **B** mixed with trivalent metal atoms in 1:1 molar ratio (see Figure 3a). A very similar topology corresponds also to the defect-free overlayer comprising linkers **I**. As shown in Figure 9b the infinite metal-organic phase ($\rho = 0.381$) is composed of large voids $(1.2.2)^6$ with diameter $d = 2\sqrt{13}$ (corner-to-corner), windmill-like pores (9 adsorption sites), and very small cavities encompassing only 2 adsorption sites. The rhombic unit cell of the considered network $\left(\sqrt{109} \times \sqrt{109}, \angle 60/120^{o}\right)$ contains 6 ligands **I** and 6 metal atoms in 1:1 stoichiometric ratio, what agree perfectly with the overall ligand/metal proportion in the system under study.

Preprints (www.preprints.org) | NOT PEER-REVIEWED | Posted: 25 March 2022 doi:10.20944/preprints202203.0340.v1

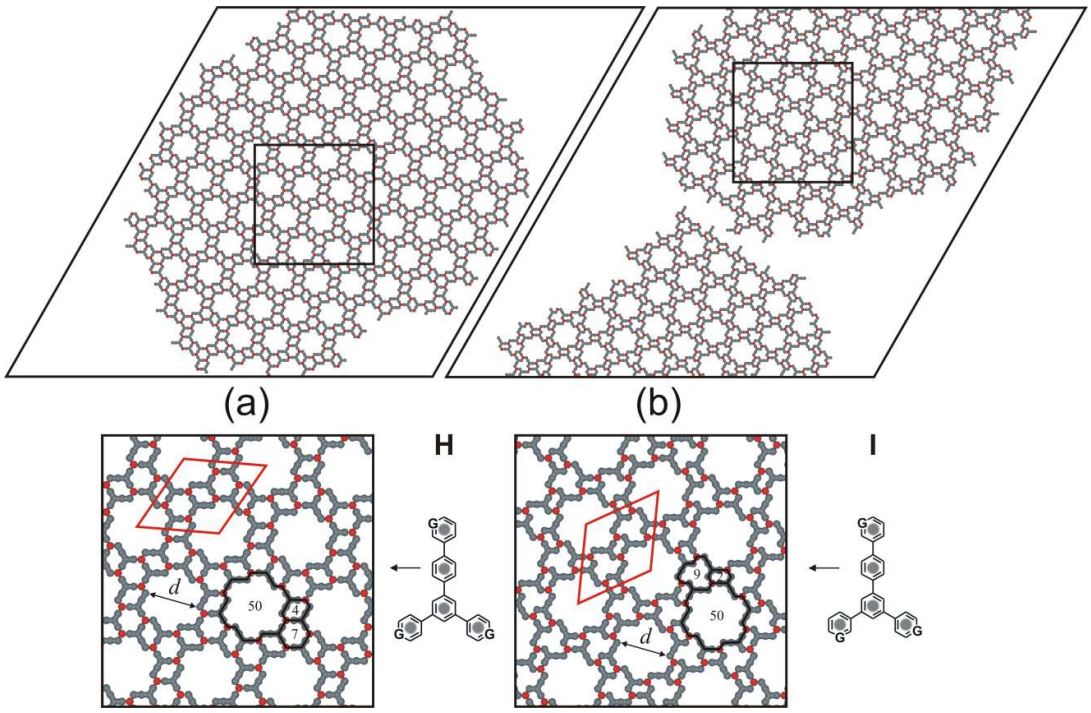

Figure 9. (**a**) A crystalline multiporous superstructure comprising 600 metal atoms and 600 ligands **H** in 1:1 stoichiometric ratio; (**b**) Openwork metal-organic phase composed of 600 metal atoms and 600 ligands **I** in 1:1 stoichiometric ratio. In the magnified fragments of the ordered metal-organic arrays the rhombic unit cells are marked (solid red lines). The solid black lines delimit the edges of empty nanopores differing in size and shape. Inside the highlighted nanopores the numbers of empty adsorption sites are given. For the largest gear-like shaped nanopores their diameters *d* (corner-to-corner) are marked.

For the last examined molecule (denoted as **J**), with arms functionalized selectively in (*S*)-*meta* positions, we have observed the formation of two polymorphs differing in terms of porosity. As it is seen in Figures 10a-b, both metal-organic networks are very similar to those obtained for achiral linker **A** (see Figures 2a-b). Namely, the multiporous overlayer shown in Figure 10a is characterized by a rhombic unit cell $\left(\sqrt{37} \times \sqrt{37}, \angle\, 60/120^{o}\right)$, comprising 3 ligands **J** and 3 trivalent metal atoms in 1:1 stoichiometric ratio. Within the open porous crystalline structure ($\rho = 0.562$) the periodically distributed windmill-like pores (9 adsorption sites) could be easily identified. Their edges are decorated by adjacent small voids enclosed 4 and 6 free adsorption sites. The second brick wall-like polymorph with a parallelogram unit cell $(3 \times 4, \angle\, 60/120^{o})$ is built of unidirectionally oriented voids including 6 adsorption sites, each (see Figure 10b). Interestingly, such close-packed arrangement of relatively small voids makes this metal-organic superstructure densest among all 2D crystals discussed in this work ($\rho = 0.577$).

Preprints (www.preprints.org) | NOT PEER-REVIEWED | Posted: 25 March 2022 doi:10.20944/preprints202203.0340.v1

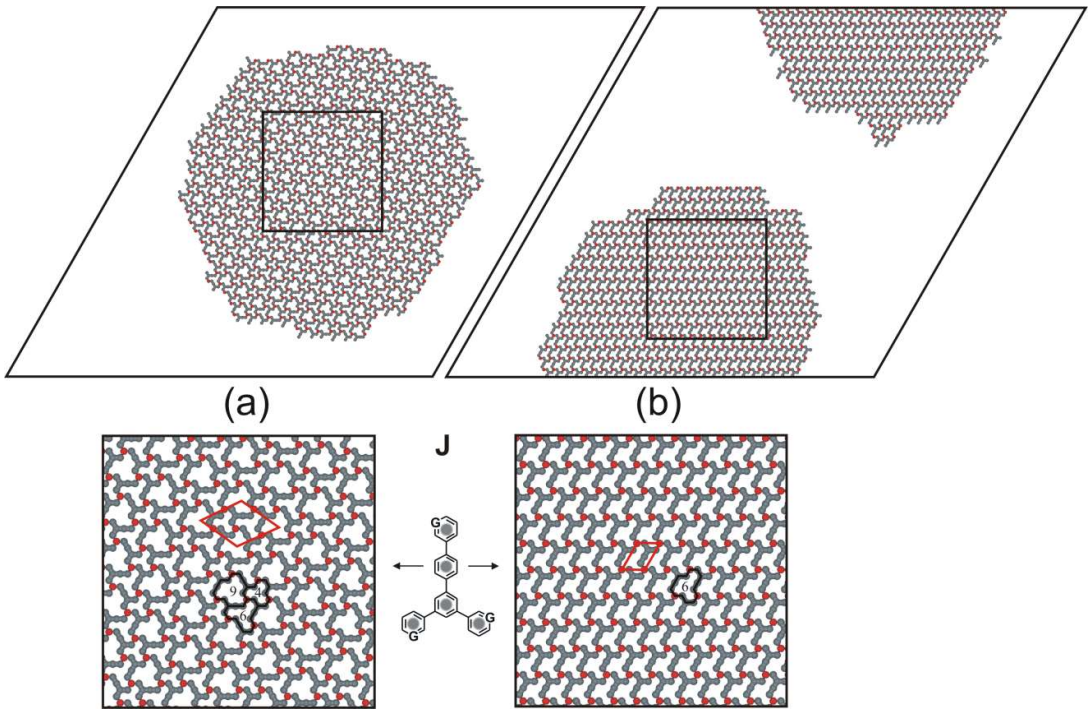

Figure 10. The polymorphic metal-organic superstructures obtained for molecule **J**. (**a**) A multiporous overlayer comprising 600 metal atoms and 600 ligands **J** in 1:1 stoichiometric ratio; (**b**) A homogenous network composed of 600 metal atoms and 600 ligands **J** in 1:1 stoichiometric ratio. In the magnified fragments of the 2D patterns the rhombic unit cells are marked (solid red lines). The solid black lines delimit the edges of empty nanopores differing in size and shape. Inside the highlighted nanopores the numbers of empty adsorption sites are given.

4. Conclusions

Exploiting the MC computer simulations we examined metal-directed self-assembly of flat π-aromatic molecules **A**-**J** with a reduced symmetry (Y-shaped backbone). The obtained theoretical results clearly indicate that the dichotomous self-assembly is a unique feature of tritopic molecules **A** and **J**, in which terminal segments (arms) are functionalized selectively in *para*/(*S*)-*meta* positions. For the surface isomers with a more complex functionalization pattern (linkers **B**, **C**, **D**, **H**, and **I**) we observed a surface-assisted formation of extended metal-organic networks with large gear-like shaped voids ($6 \leq d \leq 2\sqrt{13}$), decorated by smaller cavities differing in size and shape. Interestingly, only in the simulated system comprising linkers **E**, we observed the formation of unidirectionally oriented metal-organic ladders instead of open porous phase. However, the most intriguing supramolecular patterns corresponds to the adsorbed systems comprising ligands **F** and **G** mixed with trivalent metal atoms in 1:1 stoichiometric ratio. Surprisingly, these simple molecular building blocks were able to create complex mosaics with an aperiodic distribution of bridging linkers. To conclude, the performed MC calculations indicate that even subtle modification of intramolecular distribution of active centers embedded in termini of Y-shaped molecules strongly affects the final topology of self-assembled overlayers, where anisotropic coordination bonds play a decisive role. In this context, the investigated herein family of tritopic positional isomers may be a valuable source of molecular building blocks cementing novel surface-confined supramolecular architectures. The obtained hints could be especially useful in the surface-assisted fabricated of brand new openwork nanomaterials, metal-organic ladders, and aperiodic mosaics with high level of complexity.

Author Contributions: Conceptualization, Damian Nieckarz; Data curation, Karolina Nieckarz; Funding acquisition, Damian Nieckarz; Methodology, Damian Nieckarz; Project administration, Damian Nieckarz; Software, Karolina Nieckarz; Supervision, Damian Nieckarz; Visualization, Karolina Nieckarz; Writing – original draft, Damian Nieckarz; Writing – review & editing, Karolina Nieckarz.

Funding: This work was supported by the National Science Centre, Poland research grant: 2018/31/D/ST4/01443, SONATA 14.

Data Availability Statement: Not applicable.

Conflicts of Interest: The authors declare no conflict of interest.

References

1. Grünbaum, B.; Shephard, G. C. *Tilings and patterns*, 2nd ed.; Dover Publications, USA, 2015.
2. Schlickum, U.; Klappenberger, F.; Decker, R.; Zoppellaro, G.; Klyatskaya, S.; Ruben, M.; Kern, K.; Brune, H.; Barth, J. V. Surface-confined metal-organic nanostructures from Co-directed assembly of linear terphenyl-dicarbonitrile linkers on Ag(111). *J. Phys. Chem. C* **2010**, *114*, 15602–15606.
3. Adhikari, R.; Kuliga, J.; Ruppel, M.; Jux, N.; Marbach, H.; Steinrück, H. P. Self-assembled 2D-coordination Kagome, quadratic, and close-packed hexagonal lattices formed from a cyano-functionalized benzoporphyrin on Cu(111). *J. Phys. Chem. C* **2021**, *125*, 7204–7212.
4. Song, Y.; Wang, Y.; Jin, Q.; Zhou, K.; Shi, Z.; Liu, P. N.; Ma, Y. Self-assembly and local manipulation of Au-pyridyl coordination networks on metal surfaces. *ChemPhysChem* **2017**, *18*, 2088–2093.
5. Liu, J.; Li, J.; Xu, Z.; Zhou, X.; Xue, Q.; Wu, T.; Zhong, M.; Li, R.; Sun, R.; Shen, Z.; Tang, H.; Gao, S.; Wang, B.; Hou, S.; Wang, Y. On-surface preparation of coordinated lanthanide-transition-metal clusters. *Nat. Commun.* **2021**, *12*, 1619.
6. Song, L.; Yang, B.; Liu, F.; Niu, K.; Han, Y.; Wang, J.; Zheng, Y.; Zhang, H.; Li, Q.; Chi, L. Synthesis of two-dimensional metal-organic frameworks via dehydrogenation reactions on a Cu(111) surface. *J. Phys. Chem. C* **2020**, *124*, 12390–12396.
7. Schlickum, U.; Decker, R.; Klappenberger, F.; Zoppellaro, G.; Klyatskaya, S.; Ruben, M.; Silanes, I.; Arnau, A.; Kern, K.; Brune, H.; Barth, J. V. Metal-organic honeycomb nanomeshes with tunable Cavity size. *Nano Lett.* **2007**, *7*, 3813–3817.
8. Zhang, Y.; Zhang, X.; Li, Y.; Zhao, S.; Hou, S.; Wu, K.; Wang, Y. Packing Sierpiński triangles into two-dimensional crystals, *J. Am. Chem. Soc.* **2020**, *142*, 17928–17932.
9. Li, S. W.; Zhang, R. X.; Kang, L. X.; Li, D. Y.; Xie, Y. L.; Wang, C. X.; Liu, P. N. Steering metal-organic network structures through conformations and configurations on surfaces. *ACS Nano* **2021**, *15*, 18014–18022.
10. Bischoff, F.; He, Y.; Seufert, K.; Stassen, D.; Bonifazi, D.; Barth, J. V.; Auwärter, W. Tailoring large pores of porphyrin networks on Ag(111) by metal-organic coordination. *Chem. Eur. J.* **2016**, *22*, 15298–15306.
11. Dong, L.; Gao, Z.; Lin, N. Self-assembly of metal-organic coordination structures on surfaces. *Progr. Surf. Sci.* **2016**, *91*, 101–135.
12. Wakayama, Y. On-surface molecular nanoarchitectonics: from self-assembly to directed assembly. *Jpn. J. Appl. Phys.* **2016**, *55* 1102AA.
13. Zhang, R.; Lyu, G.; Chen, C.; Lin, T.; Liu, J.; Liu, P. N.; Lin, N. Two-dimensional superlattices of Bi nanoclusters formed on a Au(111) surface using porous supramolecular templates. *ACS Nano* **2015**, 9, 8547–8553.
14. Gutzler, R.; Stepanow, S.; Grumelli, D.; Lingenfelder, M.; Kern, K. Mimicking enzymatic active sites on surfaces for energy conversion chemistry. *Acc. Chem. Res.* **2015**, *48*, 2132–2139.
15. Li, C.; Zhang, X.; Li, N.; Wang, Y.; Yang, J.; Gu, G.; Zhang, Y.; Hou, S.; Peng, L.; Wu, K.; Nieckarz, D.; Szabelski, P.; Tang, H.; Wang, Y. Construction of Sierpiński triangles up to the fifth order. *J. Am. Chem. Soc.* **2017**, *139*, 13749–13753.
16. Liu, J.; Lin, T.; Shi, Z.; Xia, F.; Dong, L.; Liu, P. N.; Lin, N. Structural transformation of two-dimensional metal-organic coordination networks driven by intrinsic in-plane compression. *J. Am. Chem. Soc.* **2011**, *133*, 18760–18766.
17. Kumar, A.; Banerjee, K.; Foster, A. S.; Liljeroth, P. Two-dimensional band structure in honeycomb metal-organic frameworks. *Nano Lett.* **2018**, *18*, 5596–5602.
18. Umbach, T. R.; Bernien, M.; Hermanns, C. F.; Krüger, A.; Sessi, V.; Fernandez-Torrente, I.; Stoll, P.; Pascual, J. I.; Franke, K. J.; Kuch, W. Ferromagnetic coupling of mononuclear Fe centers in a self-assembled metal-organic network on Au(111). *Phys. Rev. Lett.* **2012**, *109*, 267–207.

19. Shi, Z.; Liu, J.; Lin, T.; Xia, F.; Liu, P. N.; Lin, N. Thermodynamics and selectivity of two-dimensional metallo-supramolecular self-assembly resolved at molecular scale. *J. Am. Chem. Soc.* **2011**, *133*, 6150–6153.
20. Vijayaraghavan, S.; Ecija, D.; Auwärter, W.; Joshi, S.; Seufert, K.; Drach, M.; Nieckarz, D.; Szabelski, P.; Aurisicchio, C.; Bonifazi, D.; Barth, J. V. Supramolecular assembly of interfacial nanoporous networks with simultaneous expression of metal-organic and organic-bonding motifs. *Chem. Eur. J.* **2013**, *19*, 14143–14150.
21. Ecija, D.; Vijayaraghavan, S.; Auwärter, W.; Joshi, S.; Seufert, K.; Aurisicchio, C.; Bonifazi, D.; Barth, J. V. Two-dimensional short-range disordered crystalline networks from flexible molecular modules. *ACS Nano* **2012**, *6*, 4258–4265.
22. Shu, C. H.; He, Y.; Zhang, R. X.; Chen, J. L.; Wang, A.; Liu, P. N. Atomic-scale visualization of stepwise growth mechanism of metal-alkynyl networks on surfaces. *J. Am. Chem. Soc.* **2020**, *142*, 16579–16586.
23. Yan, L.; Kuang, G.; Zhang, Q.; Shang, X.; Liu, P. N.; Lin, N. Self-assembly of a binodal metal-organic framework exhibiting a demi-regular lattice. *Faraday Discuss.* **2017**, *204*, 111–121.
24. Nijs, T.; Klein, Y. M.; Mousavi, S. F.; Ahsan, A.; Nowakowska, S.; Constable, E. C.; Housecroft, C. E.; Jung, T. A. The different faces of 4'-pyrimidinyl functionalized 4,2':6',4''-terpyridines: metal organic assemblies from solution and on Au(111) and Cu(111) surface platforms. *J. Am. Chem. Soc.* **2018**, *140*, 2933–2939.
25. Ammon, M.; Sander, T.; Maier, S. On-surface synthesis of porous carbon nanoribbons from polymer chains. *J. Am. Chem. Soc.* **2017**, *139*, 12976–12984.
26. Ammon, M.; Haller, M.; Sorayya, S.; Maier, S. On-surface synthesis of porous carbon nanoribbons on silver: reaction kinetics and the influence of the surface structure. *ChemPhysChem* **2019**, *20*, 2333–2339.
27. Šimėnas, M.; Ibenskas, A.; Tornau, E. E. Coronene molecules in hexagonal pores of tricarboxylic acids: a Monte Carlo study. *J. Phys. Chem. C* **2015**, *119*, 20524–20534.
28. Barnard, R. A.; Dutta, A.; Schnobrich, J. K.; Morrison, C. N.; Ahn, S.; Matzger, A. J. Two-dimensional crystals from reduced symmetry analogues trimesic acid. *Chem. Eur. J.* **2015**, *21*, 5954–5961.
29. Szabelski, P.; Nieckarz, D.; Rżysko, W. Influence of molecular shape and interaction anisotropy on the self-assembly of tripod building blocks on solid surfaces. *Colloids Surf. A* **2017**, *532*, 522–529.
30. Szabelski, P.; Nieckarz, D.; Rżysko, W. Structure formation in 2D assemblies comprising functional tripod molecules with reduced symmetry. *J. Phys. Chem. C* **2017**, *121*, 45, 25104–25117.
31. Gdula, K.; Nieckarz, D. On-surface self-assembly of metal-organic architectures: insights from computer simulations. *J. Phys. Chem. C* **2020**, *124*, 20066–20078.
32. Nieckarz, K.; Szabelski, P.; Nieckarz, D. Monte Carlo simulations of the self-assembly of hierarchically organized metal-organic networks on solid surfaces. *Surf. Sci.* **2022**, *719*, 122041.
33. Fadeeva, A.; Gorbunov, V. A.; Solovyeva, O. S.; Stishenko, P. V.; Myshlyavtsev, A. V. Homologous series of flower phases in metal-organic networks in Au(111) surface. *J. Phys. Chem. C* **2020**, *124*, 11506–11515.
34. Ibenskas, A.; Tornau, E. E. Modeling of high-temperature ordered structures with weak intermolecular C-H···F and C-H···N bonds. *J. Phys. Chem. C* **2021**, *125*, 19560–19569.
35. Nieckarz, D.; Szabelski, P. Simulation of the self-assembly of simple molecular bricks into Sierpiński triangle. *Chem. Comm.* **2014**, *50*, 6843–6845.
36. Lisiecki, J.; Szabelski, P. Surface-confined metal-organic precursors comprising naphthalene-like derivatives with differently distributed halogen substituents: a Monte Carlo model. *J. Phys. Chem. C* **2020**, *124*, 20280–20293.
37. Metropolis, N.; Rosenbluth, A. W.; Rosenbluth, M. N.; Teller, A. H. Equation of state calculations by fast computing machines, *J. Chem. Phys.* **1953**, *21*, 1087–1092.
38. Frenkel, D.; Smit, B. *Understanding Molecular Simulation*; Academic Press: London, U. K., 2002.
39. Lischka, M.; Michelitsch, G. S.; Martsinovich, N.; Eichhorn, J.; Rastgoo-Lahrood, A.; Strunskus, T.; Breuer, R.; Reuter, K.; Schmittel, M.; Lackinger, M. Remote functionalization in surface-assisted dehalogenation by conformational mechanics: organometallic self-assembly of 3,3′,5,5′-tetrabromo-2,2′,4,4′,6,6′-hexafluorobiphenyl on Ag(111). *Nanoscale* **2018**, *10*, 12035–12044.
40. Gutzler, R.; Cardenas, L.; Lipton-Duffin, J.; El Garah, M.; Dinca, L. E.; Szakacs, C. E.; Fu, C.; Gallagher, M.; Vondráček, M.; Rybachuk, M.; Perepichka, D. F.; Rosei, F. Ullmann-type coupling of brominated tetrathienoanthracene on copper and silver. *Nanoscale* **2014**, *6*, 2660–2668.
41. Nieckarz, D.; Rżysko, W.; Szabelski, P. On-surface self-assembly of tetratopic molecular building blocks. *Phys. Chem. Chem. Phys.* **2018**, *20*, 23363–23377.